Interfacial instability in pressure-driven core-annular pipe flow of a Newtonian and a Herschel-Bulkley fluid

R. Usha[†] and Kirti Chandra Sahu[*]
[†] *Department of Mathematics, Indian Institute of Technology Madras, Chennai 600036, India*
Department of Chemical Engineering, Indian Institute of Technology Hyderabad, Kandi, Sangareddy 502 285, Telangana, India
(Dated: July 30, 2019)

The linear stability characteristics of pressure-driven core-annular flow of a Newtonian core fluid and a Herschel-Bulkley annular fluid is investigated. The fluids are assumed to have the same density and separated by a sharp interface. The modified Orr-Sommerfeld equations for each layer are derived and solved using an efficient spectral collocation method considering a configuration without any unyielded region. The effect of various dimensionless parameters, such as the Bingham number (Bn), the flow index (n), the interface radius (R_0) and the inverse capillary number (Γ) on the instability characteristics of the flow is investigated, and an energy budget analysis is conducted to explain the physical mechanism of the instability observed. We found that axisymmetric mode is the most dominant unstable mode for the interfacial flow configuration considered in the present work, which is in contrast to miscible core-annular flows. It is observed that increasing Bn has a non-monotonic effect on the growth rate of the axisymmetric mode, and two dominant modes appear at high Bn. We found that increasing the thickness of the core fluid increases the bandwidth of the unstable wavenumbers and destabilises the short waves; however, displays a non-monotonic trend in the growth rate curves. The instability behaviour observed for different sets of parameters are investigated by conducting an energy budget analysis and analysing the disturbance eigenfunctions and the basic velocity profiles.

Keywords: Instability, Non-Newtonian fluid, core-annular flow, interfacial flow

I. INTRODUCTION

The present investigation has been motivated by the nonlinear stability analysis of Poiseuille flow of Bingham fluid in a pipe addressed by Nouar and Frigaard [1], by the analytical contribution of Moyers-Gonzalez *et al.* [2] and the computational study of lubricated core-annular flows of a viscoplastic fluid by Hormozi *et al.* [3] in the nonlinear regime. While the analysis in Ref. [1] based on an energy method for two-dimensional disturbances has predicated the critical Reynolds number below which the kinetic energy of any finite-amplitude disturbance decays monotonically in time, the stability of the flow has been established in Ref. [4] by bounding the amplitude of the shear-stress perturbation energy. Further, the eigenvalue bound for three-dimensional disturbances through a linear stability analysis was given by Frigaard and Nouar [5]. These studies have focussed on the specific flow regimes in which the surrounding fluid preserves an unyielded plug at the interface. However, there are situations when the yield stress has sufficient strength to prevent the breaking of the continuous network of the interactions between the molecules throughout the non-Newtonian fluid layer. In such cases, the plug zone may not appear and the entire layer occupied by the non-Newtonian fluid would be fully yielded. Further, it is well known and is also necessary to investigate the stability characteristics of a flow system within the framework of infinitesimal perturbations in order to have an understanding of the mechanism of laminar-turbulent transition [6]. This calls for a detailed investigation on the linear stability analysis of a core-annular lubricated flow of a viscoplastic fluid in a pipe with an annular layer hosting a fully yielded non-Newtonian fluid surrounding a Newtonian core fluid, and with this objective, the present investigation has been considered.

There has been an increased research activity in the recent years in examining the stability of immiscible and continuously stratified miscible flows of Newtonian and/or non-Newtonian fluids with different rheology, in plane channel and pipe due to their relevance in several industrial and natural applications (see for instance, Refs [7–9]). The focus in these studies has been to determine the flow regime and to understand the mechanism of shear instability in multilayer flows so as to provide information for the design of process equipments and also control the transition from laminar to turbulent state in such applications. In what follows, we present an overview of the state of the art of investigations that is close to or at the boundaries of the domain of our interest in the present study.

Several researchers have explored the stability characteristics of single layer non-Newtonian fluids in plane Couette

[*] ushar@iitm.ac.in, ksahu@iith.ac.in

and Poiseuille flows in channels and Hagen-Poiseuille flows in pipes. Frigaard *et al.* [10] studied the linear stability behaviour of two-dimensional disturbances in a plane Poiseuille flow of a Bingham fluid and have provided the formulation of the stability problem and linearisation at the yield surface. They imposed the symmetry for the eigenfunction of the vertical velocity and considered both odd and even perturbations separately.

The non-modal stability of the flow of a yield-stress fluid in a pipe has been analysed in Refs. [11, 12]. Bentrad *et al.* [13] studied the role of shear-thinning viscosity on the modal and non-modal stability analyses of a yield-stress fluid in a Hagen-Poiseuille flow configuration. The shear-thinning effect on the stability of a plane Poiseuille flow of a fluid modelled using Herschal-Bulkley model was examined by Liu *et al.* [14] via energy stability and non-modal stability methods. Their study revealed that the critical Reynolds number based on energy decreases for both the streamwise and spanwise perturbations. The optimal disturbance and the maximum energy growth are strongly influenced by the Bingham number and the shear-thinning effect.

The study of stability in multiplayer channel and pipe flows has a long history that dates back to the investigation by Yih [15] who studied the onset of interfacial instability in plane Couette-Poiseuille flow by conducting a linear stability analysis. Since then several researchers have investigated the instability in interfacial flows (see for instance, Refs. [8, 16–20]). An extensive review of the instability in viscosity-stratified systems can be found in Ref. [21] and references therein. There are also studies in core-annular configurations and other displacement flows involving Newtonian fluids (see e.g. [22–27]).

Multilayer flows involving yield-stress fluids are encountered in food processing, oil-gas industries, mineral processing, drilling and cementing of oil wells, centreline injectors, to name a few, and thus, also have attracted the attention of several researchers. These fluids have the characteristic that they behave as fluids only if the deviatoric stress exceeds the yield stress, otherwise, the rate of strain is zero and unyielded region behaves as a solid. Among the several studies on the stability of inelastic non-Newtonian fluids [4, 28, 29], the linear stability analysis of a two-layer plane Poiseuille flow of a Bingham fluid [28] motivated the study of Sahu *et al.* [20]. The normal model analysis of Ref. [28] reveals that increasing the yield stress stabilises the two-dimensional disturbances. The shear stress distribution in this study [28] is such that only a fraction of the Bingham fluid is yielded. Such a situation in a two-layer configuration gives rise to the presence of an unyielded region between the core fluid and the near-wall (Bingham) fluid, which in turn prevents the occurrence of interfacial waves, as a result the system becomes increasingly stable at bigger values of the yield stress. The conclusion of the study by Pinarbasi and Liakopoulos [30] in a two-layer flow of Carreau-Yasuda and Bingham fluids is similar to that in Ref. [28].

Sahu *et al.* [20] investigated the stability of pressure-driven two-layer channel flow of a Newtonian and a non-Newtonian fluid described by the Herschal-Bulkley constitutive equation in laminar conditions at a flow rate sufficient for the entire non-Newtonian fluid to yield (within the framework of linear stability analysis considering two-dimensional disturbances). Thus, their analysis was away from the critical condition for the onset of an unyielded region to form. In addition to being relevant in a number of applications where the applied pressure-gradient is very large, the study in Ref. [20] shows that when the non-Newtonian layer is yielded completely, the Bingham number destabilises the two-layer channel flow. Later, they have extended this study to investigate the behaviour of three-dimensional disturbances and found that three-dimensional disturbances are more unstable than the two-dimensional ones [8] and also identified the parameters for which the two-layer flow becomes absolutely unstable [31].

Recently, Sahu [32] conducted a linear stability study of miscible core-annular flow of a Bingham fluid (as the annular fluid) and a Newtonian fluid (as the core fluid) in a cylindrical pipe. The normal-mode analysis of three-dimensional disturbances under the parallel flow assumption reveals that for the case when the non-Newtonian fluid is completely yielded, the corkscrew mode is more unstable than the corresponding axisymmetric mode and that the Bingham number destabilises the dominant corkscrew mode via an inviscid mechanism. The critical Reynolds number for the linear instability was also found to be decreased with the increase in the Bingham number for the corkscrew mode. However, they observed stable flow for low Bingham numbers in case of the axisymmetric mode. The energy due to the gradient of viscosity perturbation in the radial direction, and the transfer of energy from the basic flow to the perturbation via the "Reynolds stress" term were found to be responsible for the instability in the miscible core-annular configuration considered by Sahu [32]. Frigaard *et al.* [10] and Hormozi *et al.* [3] have shown that the flow is stable in the presence of unyielded region. Apart from the experimental studies of the instability of non-Newtonian immiscible fluids in cylindrical pipes [11, 33–36], instabilities in core-annular flows of immiscible fluids have also been studied using energy stability methods [3, 4, 29, 37–39]. The nonlinear perturbations of an axisymmetric basic flow have been analysed in Refs. [4, 38], in which a circular region of core fluid (Newtonian [2] and viscoelastic [38]) is surrounded concentrically by an annular yield-stress fluid. Three different types of basic flows have been presented accordingly as whether or not the Bingham fluid moves at all and whether or not the Bingham fluid is yielded at the interfacial region. In the first case, the focus has been on the nonlinear stability of the basic flow for which there exists an unyielded plug surrounding the core fluid using the energy stability approach. The other two cases correspond to the entirely yielded Bingham fluid and when the Bingham fluid is fully unyielded and does not flow. Their results reveal that the disturbed flow does not decay to the axisymmetric base flow but

decays to a base flow having a Newtonian core encapsulated within the Bingham fluid surrounded by a ring of fluid that is unyielded. By conducting experiments, Huen *et al.* [37] reported that when stable flow are observed, they are axisymmetric. Kindled by the curiosity to explore and understand the stability characteristics in a core-annular configuration where the passage of the core Newtonian fluid is lubricated by a shear-thinning yield-stress fluid (using the Herschal-Bulkley constitutive model), when the non-Newtonian fluid is entirely yielded, that has not been given any attention so far, has been considered in the present study. Thus, the objective of the present work is to examine the interfacial instability in immiscible core-annular flow of a shear-thinning, yield-stress fluid (annular fluid) and Newtonian fluid (core fluid) in a cylindrical pipe. A linear stability analysis of a laminar basic state in which the non-Newtonian layer is completely yielded, i.e far away from the criticality, is performed and the growth rate of the unstable waves is analysed for different parameters. The study on the flow conditions close to the critical value of the Bingham number, beyond which unyielded region forms, will be considered in future. An energy budget analysis is conducted to explain the physical mechanism of the instability characteristics observed in the present study.

The paper is organised as follows. The mathematical formulation and the governing linearised stability equations for the amplitudes of the perturbations are presented in Section II. The effects of the Bingham number and shear-thinning nature of the annular fluid are investigated through a parametric study and are presented in Section III. The energy budget analysis is presented for typical situations in this section. Finally, in Section IV, the concluding remarks are provided.

II. FORMULATION

We consider linear instability of pressure-driven core-annular flow of two immiscible incompressible fluids in a cylindrical pipe of radius R. The core and annular fluids are designated as fluid '1' and fluid '2', respectively. A schematic diagram of the flow configuration is shown in Fig. 1. A cylindrical coordinate system (r, θ, z), where r, θ and z denote the radial, the azimuthal and the axial coordinates, respectively, is used. The core fluid (fluid '1') located in the region $0 \leq r \leq R_0$ is a Newtonian fluid of viscosity μ_1, whereas the annular fluid (fluid '2') located in the region $R_0 \leq r \leq R$ is a non-Newtonian fluid of viscosity μ_2. The densities of fluid '1' and fluid '2' are designated by ρ_1 and ρ_2, respectively.

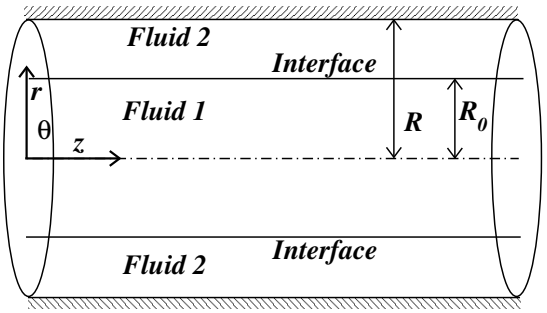

FIG. 1: Schematic of the basic flow configuration considered. Two immiscible fluids, fluid '1' and fluid '2' occupy the core $(0 \leq r \leq R_0)$ and annular $(R_0 \leq r \leq R)$ regions of the pipe, respectively.

We adopt the Herschel-Bulkley model [20] to describe the rheological characteristics of the non-Newtonian fluid (fluid '2'), which is given by

$$\mu_2 = k\Pi^{n-1} + \tau_0\Pi^{-1}, \tag{1}$$

where k and n denote the consistency and flow index, respectively, τ_0 is the yield shear stress and $\Pi = (2E_{ij}E_{ij})^{1/2}$ represents the second invariant of the rate of strain tensor. In expanded form,

$$\Pi^2 = \Big\{2\Big[\Big(\frac{\partial u_{r,2}}{\partial r}\Big)^2 + \Big(\frac{1}{r}\frac{\partial u_{\theta,2}}{\partial \theta} + \frac{u_{r,2}}{r}\Big)^2 + \Big(\frac{\partial u_{z,2}}{\partial z}\Big)^2\Big] + \Big[r\frac{\partial}{\partial r}\Big(\frac{u_{\theta,2}}{r}\Big) + \frac{1}{r}\frac{\partial u_{r,2}}{\partial \theta}\Big]^2 + \Big[\frac{\partial u_{r,2}}{\partial r} + \frac{\partial u_{z,2}}{\partial r}\Big]^2 + \Big[\frac{1}{r}\frac{\partial u_{z,2}}{\partial \theta} + \frac{\partial u_{\theta,2}}{\partial z}\Big]^2\Big\}, \tag{2}$$

The flow dynamics is governed by the incompressible form of the continuity and the Navier-Stokes equations in the cylindrical coordinate system. The following scalings are employed to render the governing equations dimensionless:

$$(r, z, R_0) = R\left(\widetilde{r}, \widetilde{z}, \widetilde{R}_0\right),\ t = \frac{R}{V}\widetilde{t},\ (u_{r,i}, u_{\theta,i}, u_{z,i}) = V\left(\widetilde{u}_{r,i}, \widetilde{u}_{\theta,i}, \widetilde{u}_{z,i}\right),\ p_i = \rho V^2 \widetilde{p}_i,\ \rho_i = \widetilde{\rho}_i\rho_1,\ \mu_i = \widetilde{\mu}_i\mu_1, \tag{3}$$

where $V\left(\equiv Q/\pi R^2\right)$ is the average inlet velocity; $u_{r,i}$, $u_{\theta,i}$ and $u_{z,i}$ are the components of the velocity in the the radial, the azimuthal and the axial directions, respectively; t denotes time; ρ_i represents density; p_i denotes pressure. Here the subscripts $(i = 1, 2)$ represent the flow quantities associated with fluid '1' and '2', respectively. In Eq. (3), tildes designate dimensionless quantities, which are dropped hereafter.

The dimensionless governing equations are given by

$$\nabla \cdot \mathbf{u}_i = 0, \tag{4}$$

$$\rho_i \left[\frac{\partial \mathbf{u}_i}{\partial t} + \mathbf{u}_i \cdot \nabla \mathbf{u}_i\right] = -\nabla p_i + \frac{1}{Re}\nabla \cdot \left[\mu_i(\nabla \mathbf{u}_i + \nabla \mathbf{u}_i^T)\right], \tag{5}$$

where $\mathbf{u}_i\,(\equiv (u_{r,i}, u_{\theta.i}, u_{z,i}))$ is the velocity field, $Re(\equiv \rho_1 V R/\mu_1)$ is the Reynolds number. The dimensionless density and viscosity of fluid '1' are unity, and the dimensionless density of fluid '2' is $\rho_r(\equiv \rho_2/\rho_1)$, which is the density ratio between the fluids. In what follows, we consider fluids with matched density in the two layers ($\rho_i = 1$), so as to eliminate the buoyancy effect.

The dimensionless viscosity of the non-Newtonian fluid, μ_2 is given by

$$\mu_2 = m|\Pi|^{n-1} + Bn|\Pi|^{-1}, \tag{6}$$

where $Bn\,(\equiv \tau_0 R/\mu_1 V)$ and $m(\equiv k\mu_1^{-1}\,(V/R)^{n-1})$ are the Bingham number and the Newtonian viscosity ratio, respectively.

A. Basic state

In this section, we derive the basic state in the core-annular flow configuration, whose linear stability characteristic will be analysed. The annular and the core regions host a non-Newtonian fluid and a Newtonian fluid, respectively. The fluids are assumed to be incompressible. The basic state flow variables are designated by upper-case letters and basic state viscosity of the the non-Newtonian annular fluid by μ_2^0. A pressure-gradient is applied along the axis of the pipe. The basic state velocity profile is a steady, parallel, fully-developed unidirectional flow along the axis of the pipe, i.e., $U_{r,i} = U_{\theta,i} = 0$; $U_{z,i} = U_{z,i}(r)$, i=1,2, and $P = P_1 = P_2$ is a linear function of z. We focus on the situation where the basic flow in the non-Newtonian layer is fully yielded, i.e. the velocity gradient is non-zero except at $r = 0$. Thus, the equations associated with the basic state for both layers are given as follows.

For Newtonian fluid layer (fluid '1', $r \in [0, R_0]$):

$$\frac{1}{r}\frac{\partial}{\partial r}\left[r\frac{\partial U_{z,1}}{\partial r}\right] = \frac{dP}{dz}Re, \tag{7}$$

and for non-Newtonian fluid layer (fluid '2', $r \in [R_0, 1]$):

$$\frac{1}{r}\frac{\partial}{\partial r}\left[r\mu_2^0\frac{\partial U_{z,2}}{\partial r}\right] = \frac{dP}{dz}Re. \tag{8}$$

Eqs. (7) and (8) are solved using the no-slip boundary condition at the pipe wall ($r = 1$), the condition that the velocity remains bounded at the centerline of the pipe ($r = 0$), and the continuity of velocities ($U_{z,1} = U_{z,2}$) and the shear stresses ($\mu_2^0\frac{\partial U_{z,2}}{\partial r} = \frac{\partial U_{z,1}}{\partial r}$) at the interface ($r = R_0$). The pressure gradient dP/dz is calculated by maintaining a constant volumetric flow condition, such that dimensionless average velocity, $V = Q/2\pi\int_0^1 r dr = 1$, i.e.

$$\int_0^{R_0} U_{z,1} r dr + \int_{R_0}^1 U_{z,2} r dr = \frac{1}{2}. \tag{9}$$

As our focus is on the scenario when the non-Newtonian layer is fully-yielded, a condition on the location, R_0 of the interface, for a given set of values of Bn, n and m can be obtained by requiring that $\Pi = 0$ in the annular layer; in the basic state, $\Pi = \frac{dU_{z,2}}{dr}$, and is given by

$$\Pi = \frac{1}{m^{1/n}}\left[\frac{r}{2}\left|\frac{dP}{dz}\right| Re - Bn\right]^{1/n}. \tag{10}$$

$\Pi = 0$ gives the 'yield surface' as

$$y_s = \frac{2Bn}{\left|\frac{dP}{dz}\right| Re}, \tag{11}$$

where $|\frac{dP}{dz}|$ is obtained from Eq. (9). By taking $y_s = R_0$, the numerical results are obtained by choosing the parameters in such a way that the condition

$$1 > R_0 > \frac{2Bn}{|\frac{dP}{dz}|\, Re}, \tag{12}$$

is satisfied.

From Eqs. (7) and (8), the basic velocity profiles in the two layers are

$$U_{z,1} = \left|\frac{dP}{dz}\right| \frac{Re}{4}({R_0}^2 - r^2) + \frac{2n}{n+1} \frac{1}{|\frac{dP}{dz}|\,(Re) m^{1/n}} \left[\left(\left|\frac{dP}{dz}\right| \frac{Re}{2} - Bn \right)^{\frac{n+1}{n}} - \left(\left|\frac{dP}{dz}\right| \frac{ReR_0}{2} - Bn \right)^{\frac{n+1}{n}} \right], \tag{13}$$

$$U_{z,2} = \frac{2n}{n+1} \frac{1}{|\frac{dP}{dz}|\,(Re) m^{1/n}} \left[\left(\left|\frac{dP}{dz}\right| \frac{Re}{2} - Bn \right)^{\frac{n+1}{n}} - \left(\left|\frac{dP}{dz}\right| \frac{Re}{2} r - Bn \right)^{\frac{n+1}{n}} \right]. \tag{14}$$

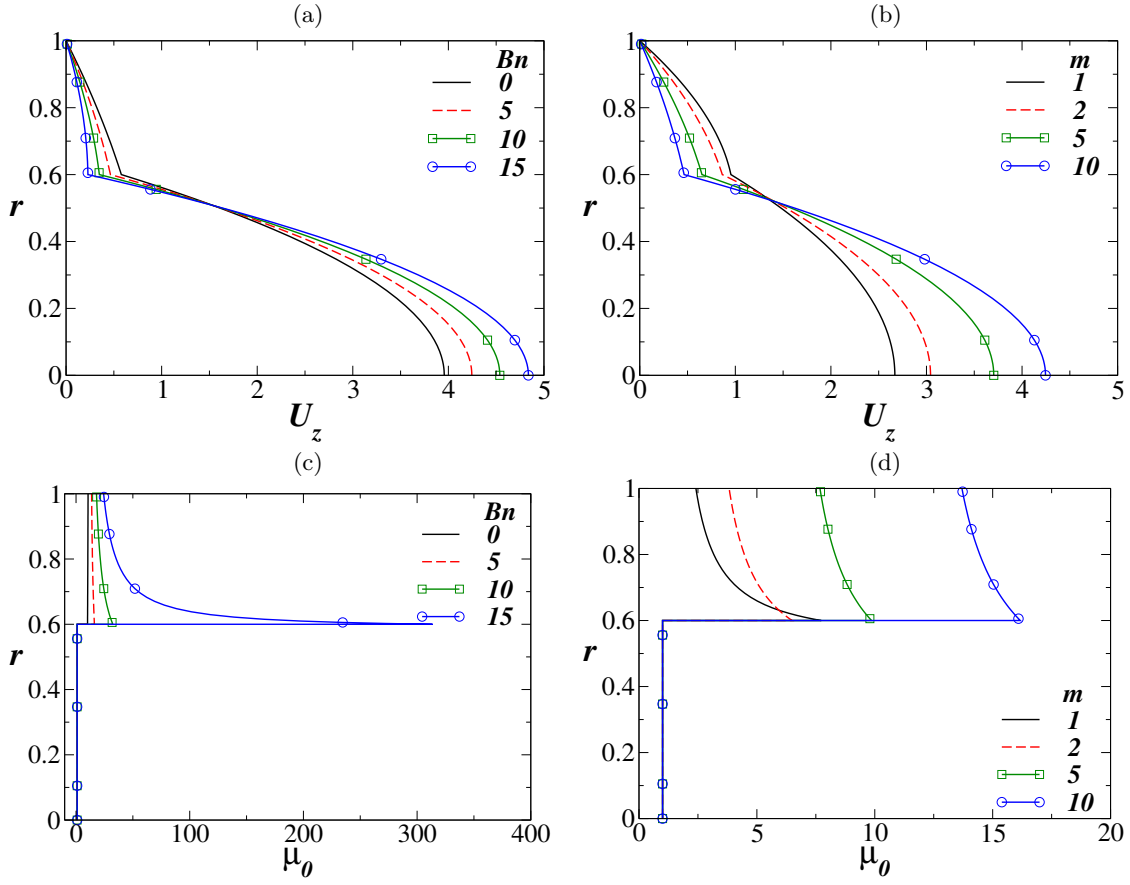

FIG. 2: Basic state profiles of (a,b) axial velocity (U_z) and (c,d) viscosity (μ_0), (a,c) Effect of Bn for $m = 10$ and (b,d) effect of m for $Bn = 5$. The rest of the parameter values are $R_0 = 0.6$ and $n = 1.1$.

The basic state profiles of the axial velocity ($U_{z,i}$) and viscosity (μ_0) are plotted in Fig. 2 with $m = 10$ for different values of the Bingham number (panels (a) and (c)) and with $Bn = 5$ for different values of m (panels (b) and (d)). The rest of the parameter values are $R_0 = 0.6$ and $n = 1.1$. It can be seen that as Bn increases, the axial velocity at the centerline increases and the trend persists till a certain location in the radial direction, within the Newtonian layer (Fig. 2a) for $m = 10$. This corresponds to a decrease in the axial velocity gradient (U_z') in the Newtonian layer as Bn increases. In a region near to the interface, a reverse trend is seen as Bn increases and this gives rise to an increase in U_z' in this region. However, for a fixed Bn, there is a decrease in U_z in both the Newtonian core and the non-Newtonian annular layers. In the non-Newtonian layer, U_z increases with the increase in Bn, which results in a

decrease in U_z'. This may attributed to the increase in shear in this layer. This is associated with a steep increase in μ_0 at the interface in the non-Newtonian layer (see $Bn = 15$ in Fig. 2(c), which then decreases gradually with increasing r. As Bn increases, the viscosity increases along the radial direction in the non-Newtonian layer as one moves from the interface towards the pipe wall. For fixed Bn and fixed m, the axial velocity in the Newtonian core is larger than that at the interface and in the non-Newtonian layer. The difference in the maximum axial velocity between the lower layer and the upper layer increases with the increase in Bn, as well as, with the increase in m.

For a fixed value of Bn ($Bn = 5$), a decrease in the viscosity ratio (m) decreases the axial velocity at the centerline and in the Newtonian core (Fig. 2b). In the annular layer, increase in m decreases the axial velocity U_z. For a fixed value of m, U_z decreases in both the layers as one moves from the centerline to the wall of the pipe, lubricated by the non-Newtonian fluid. For $Bn = 5$, the viscosity (μ_0) decreases with decrease in m at the interface as well as in the non-Newtonian layer. This indicates that in the lubricating non-Newtonian annular layer near the wall, the viscosity μ_0 increases and the velocity gradient decreases due to the modification in the viscosity stratification and the wall-shear rate effected by an increase in the Bingham number, Bn and the viscosity ratio, m. It is clear from the above discussion that apart from the location of the interface (R_0) and the flow index (n), the interfacial instability in this core-annular system will be greatly influenced by the Bingham number (Bn), which is a measure of the viscoplasticity of the fluid and the viscosity ratio, m. In what follows, we shall focus our attention on the roles of Bn, R_0 and n on the instability characteristics of the system when $m = 10$.

B. Linear stability equations

We investigate the temporal stability characteristics of the basic flow given by Eqs (13)-(14) to infinitesimal perturbations using a normal mode analysis by expressing each flow variable as a sum of the basic state and a time-dependent perturbation (designated by a hat):

$$(\mathbf{u}_{r,i}, \mathbf{u}_{\theta,i}, \mathbf{u}_{z,i}, p_i)(r,\theta,z,t) = (0, 0, U_{z,i}(r), P) + (\mathrm{i}\hat{u}_{r,i}, \hat{u}_{\theta,i}, \hat{u}_{z,i}, \hat{p}_i)(r,\theta,z,t), \tag{15}$$

Similarly for viscosity of fluid '2', μ_2, we have

$$\mu_2(\pi) = \mu_2^0 + \tfrac{\partial \mu_2}{\partial \pi}|^0(\pi - \Pi) \equiv \mu_2^0 + S_0\hat{\pi} \equiv \mu_2^0 + \hat{\mu},$$

where

$$\begin{aligned} (\mathrm{i}\hat{u}_{r,i}, \hat{u}_{\theta,i}, \hat{u}_{z,i}, \hat{p}_i) &= (\mathrm{i}u_{r,i}, u_{\theta,i}, u_{z,i}, p_i)(r)e^{\mathrm{i}(\alpha z + \beta\theta - \omega t)}. \\ \hat{\mu} &= \mu(r)e^{\mathrm{i}(\alpha z + \beta\theta - \omega t)}. \end{aligned} \tag{16}$$

The perturbed interface can be represented as $R_0 + \hat{r}_0(z,\theta,t)$, where

$$\hat{r}_0(z,\theta,t) = r_0 e^{\mathrm{i}(\alpha z + \beta\theta - \omega t)}. \tag{17}$$

Here $S_0 \equiv (\partial\mu_2/\partial\pi)|^0 = (n-1)m|\Pi|^{n-2} - Bn|\Pi|^{-2}$; $\mathrm{i} \equiv \sqrt{-1}$, α, β and $\omega(\equiv \alpha c)$ are the wavenumbers in the axial and the azimuthal directions (real), and the frequency (complex) of the perturbation, respectively, wherein $c(\equiv c_r + \mathrm{i}c_i)$ is the phase speed of the perturbation. The subscripts r and i represent the real and imaginary parts, respectively. Here, a given mode is unstable if $\omega_i > 0$, stable if $\omega_i < 0$ and neutrally stable if $\omega_i = 0$.

Following the standard procedure [40]: (i) substitution of Eq. (16) into Eqs. (4)-(5), (ii) subtraction of the basic state equations, and (iii) linearization and elimination of the pressure perturbation, we obtained the following linear stability equations (suppressing the hat notations) for each layer.

For Newtonian fluid layer (fluid '1'):

$$u_{r,1}' + \frac{u_{r,1}}{r} + \frac{\beta u_{\theta,1}}{r} + \alpha u_{z,1} = 0, \tag{18}$$

$$-\omega u_{r,1} + \alpha u_{r,1}U_{z,1} = p_1' - \frac{\mathrm{i}}{Re}\left[u_{r,1}'' + \frac{u_{r,1}'}{r} - \left(\frac{\beta^2+1}{r^2} + \alpha^2\right)u_{r,1} - \frac{2\beta}{r^2}u_{\theta,1}\right], \tag{19}$$

$$-\omega u_{\theta,1} + \alpha u_{\theta,1}U_{z,1} = -\frac{\beta p_1}{r} - \frac{\mathrm{i}}{Re}\left[u_{\theta,1}'' + \frac{u_{\theta,1}'}{r} - \left(\frac{\beta^2+1}{r^2} + \alpha^2\right)u_{\theta,1} - \frac{2\beta}{r^2}u_{r,1}\right], \tag{20}$$

$$-\omega u_{z,1} + U'_{z,1} u_{r,1} + \alpha U_{z,1} u_{z,1} = -\alpha p_1 - \frac{\mathrm{i}}{Re}\left[u''_{z,1} + \frac{u'_{z,1}}{r} - \left(\frac{\beta^2}{r^2} + \alpha^2\right) u_{z,1}\right], \tag{21}$$

For non-Newtonian fluid layer (fluid '2'):

$$u'_{r,2} + \frac{u_{r,2}}{r} + \frac{\beta u_{\theta,2}}{r} + \alpha u_{z,2} = 0, \tag{22}$$

$$-\omega u_{r,2} + \alpha u_{r,2} U_{z,2} = p'_2 - \frac{\mathrm{i}}{Re}\Big[\mu_2^0\left\{u''_{r,2} + \frac{u'_{r,2}}{r} - \left(\frac{\beta^2+1}{r^2} + \alpha^2\right) u_{r,2} - \frac{2\beta}{r^2} u_{\theta,2}\right\} +$$

$$2\mu_0^{2\prime} u'_{r,2} + \alpha U'_{z,2}\mu\Big], \tag{23}$$

$$-\omega u_{\theta,2} + \alpha u_{\theta,2} U_{z,2} = -\frac{\beta p_2}{r} - \frac{\mathrm{i}\mu_2^0}{Re}\left\{u''_{\theta,2} + \frac{u'_{\theta,2}}{r} - \left(\frac{\beta^2+1}{r^2} + \alpha^2\right) u_{\theta,2} - \frac{2\beta}{r^2} u_{r,2}\right\} -$$

$$\frac{\mathrm{i}\mu_2^{0\prime}}{Re}\left[u'_{\theta,2} - \frac{u_{\theta,2}}{r} - \frac{\beta u_{r,2}}{r}\right], \tag{24}$$

$$-\omega u_{z,2} + U'_{z,2} u_{r,2} + \alpha U_{z,2} u_{z,2} = -\alpha p_2 - \frac{\mathrm{i}\mu_2^0}{Re}\left\{u''_{z,2} + \frac{u'_{z,2}}{r} - \left(\frac{\beta^2}{r^2} + \alpha^2\right) u_{z,2}\right\} -$$

$$\frac{\mathrm{i}\mu_2^{0\prime}}{Re}\left[u'_{z,2} - \alpha u_{r,2}\right] - \frac{\mathrm{i}U'_{z2}}{Re}\mu' - \frac{\mathrm{i}\mu}{Re}\left[U''_{z,2} + \frac{U'_{z,2}}{r}\right], \tag{25}$$

where the prime denotes differentiation with respect to r. Solutions of these equations are obtained subject to the following boundary conditions [26, 41]. The presence of the Herschel-Bulkley fluid in the annular region can affect the linear stability of the flow due to additional terms appearing in the right hand side of Eqs. (23) - (25), which correspond to contribution to the viscous stresses. Further, the inertial terms are affected by the basic velcity profile, which depends on Bn and n.

At the centerline of the pipe ($r = 0$), the boundary conditions are

$$u_{r,1} = 0, \;\; u_{\theta,1} = 0, \;\; u'_{z,1} = 0, \;\; p'_1 = 0 \;\; \text{for} \;\; \beta = 0, \tag{26}$$

$$u_{r,1} + u_{\theta,1} = 0, \;\; 2u'_{r,1} + u'_{\theta,1} = 0, \;\; u_{z,1} = 0, \;\; p_1 = 0, \;\; \text{for} \;\; \beta = 1, \tag{27}$$

$$u_{r,1} = 0, \;\; u_{\theta,1} = 0, \;\; u_{z,1} = 0, \;\; p_1 = 0, \;\; \text{for} \;\; \beta \geq 2. \tag{28}$$

At the pipe wall ($r = 1$), the boundary conditions are

$$u_{r,2} = 0, \;\; u_{\theta,2} = 0, \;\; u_{z,2} = 0, \tag{29}$$

for all values of β. The two tangential and one normal stress balance boundary conditions at $r = R_0$ are given by

$$\mu_2^0\left[-\beta u_{r,2} + R_0 u'_{\theta,2} - u_{\theta,2}\right] + \left[\beta u_{r,1} - R_0 u'_{\theta,1} + u_{\theta,1}\right] = 0, \tag{30}$$

$$\mu_2^0\left[-\alpha u_{r,2} + r_0 U''_{z,2} - u'_{z,2}\right] + \left[\mu^{0\prime}{}_2 r_0 + \mu\right] U'_{z,2} = -\alpha u_{r,1} + r_0 U''_{z,1} + u'_{z,1}, \tag{31}$$

$$Re(p_1 - p_2) + 2\mathrm{i}\left[\mu_2^0 u'_{r,2} - u'_{r,1}\right] - 2\mathrm{i}\alpha r_0\left[\mu_2^0 U'_{z,2} - U'_{z,1}\right] = -\frac{\Gamma r_0}{R_0^2}\left[1 - \beta^2 - \alpha^2 R_0^2\right], \tag{32}$$

where $\Gamma\,(\equiv \sigma/\mu_1 V)$ is the inverse capillary number.

The velocity components are also continuous at the interface ($r = R_0$), i.e.

$$u_{r,1} = u_{r,2}, \tag{33}$$
$$u_{\theta,1} = u_{\theta,2}, \tag{34}$$
$$u_{z,1} = u_{z,2}. \tag{35}$$

In addition to this, the kinematic boundary condition gives

$$r_0 = \frac{u_{r,1}}{\alpha U_{z,1} - \omega} = \frac{u_{r,2}}{\alpha U_{z,2} - \omega}. \tag{36}$$

Eqs. (18) − (25), along with the boundary conditions (29)-(36) constitute an eigenvalue problem with eigenvalue as the frequency of the disturbance (ω) and eigenvectors $[u_{r,1}, u_{\theta,1}, u_{z,1}, p_1, u_{r,2}, u_{\theta,2}, u_{z,2}, p_2]^T$.

The domains $[0, R_0]$ and $[R_0, 1]$ are discretized using Chebyshev spectral collocation method [42], and the eigenvalue problem is solved using a public domain software, LAPACK, such that for domain $[0, R_0]$:

$$r_j = R_0 \left[1 - cos\left(\frac{\pi(j-1)}{N-1}\right)\right], \tag{37}$$

and for domain $[R_0, 1]$

$$r_j = \frac{1}{2}\left[1 + cos\left(\frac{\pi(j-1)}{N-1}\right)\right] + \frac{R_0}{2}\left[1 - cos\left(\frac{\pi(j-1)}{N-1}\right)\right], \tag{38}$$

where r_j are the locations of the Chebyshev collocation points, and N is the number of collocation points in each layer.

C. Validation

In order to validate the present linear stability solver, comparisons with several published results for single fluid flow of Newtonian fluid in a pipe (the Hagen-Poiseuille flow) and core-annular flows of Newtonian and non-Newtonian fluids have been conducted. We compare (not shown) the eigenspectrums for the Hagen-Poiseuille flow obtained using the present code with those given in Ref. [40] for different values of axial and azimuthal wavenumbers and obtain excellent agreement. The results obtained from the miscible version of the present solver is also compared with the linear stability result of miscible core-annular flow through a straight pipe by Selvam *et al.* [26]. These validation exercises were presented in our previous papers [32, 43] and thus have been excluded here to avoid repetition. However, a grid convergence test has been conducted for a typical set of parameters in Fig. 3, where the dispersion curves (ω_i versus α) obtained using different number of collocation points are presented. It can be seen that the results obtained using different collocation points are virtually indistinguishable. Thus, the rest of the results are generated using the intermediate level of grid refinement ($N = 61$). However, for most of the cases, the results are also verified using higher number of collocation points.

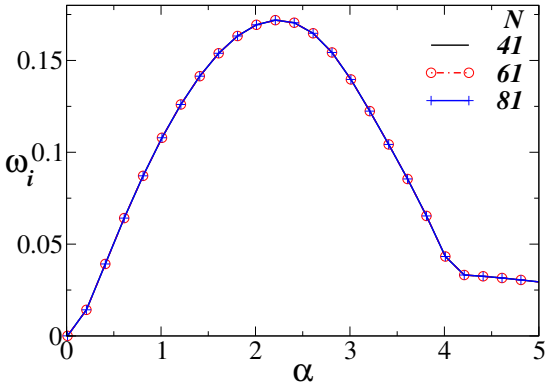

FIG. 3: Grid convergence test showing the dispersion curves (ω_i versus α) obtained using different values of N. The rest of the parameter values are $Re = 50$, $Bn = 5$, $m = 2$, $\Gamma = 5$, $\beta = 0$, $R_0 = 0.6$ and $n = 1.2$.

D. Energy budget analysis

An energy budget analysis is conducted for understanding the physical mechanism underlying the instabilities observed in the immiscible core-annular pipe flow of a Newtonian and a Herschel-Bulkley fluid. The derivation is similar to those presented for miscible flow systems in a pipe involving Newtonian [26] and non-Newtonian fluid [32]. A similar study was also conducted to understand the double-diffusive instability in a two-dimensional channel [43, 44]. Following the standard procedure [45], i.e by taking the dot product of the velocity vector with the disturbance equations (Eqs. (18)-(25)) and integrating across the domain ($0 < r < 1$), we obtained the energy budget equation, which is given by

$$2\omega_i \mathcal{E} = \mathcal{P} + \mathcal{D} + \mathcal{I} + \mathcal{V}_{vis} + \mathcal{V}_g + \mathcal{B}_r + \mathcal{V}_p, \tag{39}$$

where $\mathcal{E}$ is the temporal rate of change of the perturbation kinetic energy; $\mathcal{P}$ represents the "Reynolds stress" term which denotes the rate of energy transfer from the basic flow to the perturbations; $\mathcal{D}$ denotes the viscous dissipation of perturbation energy; $\mathcal{I}$ is the rate of work done at the interface due to interfacial forces; $\mathcal{V}_{vis}$ is the rate of work done by the basic state viscosity; $\mathcal{V}_G$ represents the rate of work done due to mean viscosity gradient; $\mathcal{B}_r$ is the rate of work done by the gradient of viscosity perturbation in the radial direction; $\mathcal{V}_p$ rate of work done due to the pressure gradient. They are given by

$$\begin{aligned}\mathcal{E} &= \frac{1}{2}\int_0^{R_0}\left(u_{r,1}u_{r,1}^* + u_{\theta,1}u_{\theta,1}^* + u_{z,1}u_{z,1}^*\right) r dr \\ &+ \frac{1}{2}\int_{R_0}^{1}\left(u_{r,2}u_{r,2}^* + u_{\theta,2}u_{\theta,2}^* + u_{z,2}u_{z,2}^*\right) r dr,\end{aligned} \tag{40}$$

$$\mathcal{P} = \int_0^{R_0} \mathrm{Imag}\left(u_{r,1}u_{z,1}^*\right) U_{z,1}' r dr + \rho_r \int_{R_0}^{1} \mathrm{Imag}\left(u_{r,2}u_{z,2}^*\right) U_{z,2}' r dr, \tag{41}$$

$$\begin{aligned}\mathcal{D} &= -\frac{1}{Re}\int_0^{R_0}\Big[u_{r,1}'{u_{r,1}'}^* + u_{\theta,1}'{u_{\theta,1}'}^* + u_{z,1}'{u_{z,1}'}^* \\ &+ \left(\frac{\beta^2}{r^2}+\alpha^2\right)\left(u_{r,1}u_{r,1}^* + u_{\theta,1}u_{\theta,1}^* + u_{z,1}u_{z,1}^*\right) + \frac{1}{r^2}\left\{u_{r,1}u_{r,1}^* + u_{\theta,1}u_{\theta,1}^*\right\}\Big] r dr \\ &- \frac{\mu_2^0}{Re}\int_{R_0}^{1}\Big[\left(u_{r,2}'{u_{r,2}'}^* + u_{\theta,2}'{u_{\theta,2}'}^* + u_{z,2}'{u_{z,2}'}^*\right) \\ &+ \left(\frac{\beta^2}{r^2}+\alpha^2\right)\left(u_{r,2}u_{r,2}^* + u_{\theta,2}u_{\theta,2}^* + u_{z,2}u_{z,2}^*\right) + \frac{1}{r^2}\left(u_{r,2}u_{r,2}^* + u_{\theta,2}u_{\theta,2}^*\right)\Big] r dr,\end{aligned} \tag{42}$$

$$\begin{aligned}\mathcal{I} &= -\mathrm{Imag}\Big[\frac{R_0}{Re}u_{r,1}^*\Big|_{R_0}\Big\{-\frac{\Gamma r_0}{{R_0}^2}\left(1-\beta^2-\alpha^2{R_0}^2\right) - 2\mathrm{i}\left(\mu_2^0 u_{r,2}' - u_{r,1}'\right) \\ &+ 2\mathrm{i}\alpha r_0\left(\mu_2^0 U_{z,2}' - U_{z,1}'\right)\Big\}\Big|_{R_0}\Big] + \mathrm{Imag}\left[\frac{\mathrm{i}R_0}{Re}\left(u_{r,1}'u_{r,1}^* + u_{\theta,1}'u_{\theta,1}^* + u_{z,1}'u_{z,1}^*\right)\right]_{R_0} \\ &- \mathrm{Imag}\left[\frac{\mathrm{i}R_0\mu_2^0}{Re}\left(u_{r,2}'u_{r,2}^* + u_{\theta,2}'u_{\theta,2}^* + u_{z,2}'u_{z,2}^*\right)\right]_{R_0},\end{aligned} \tag{43}$$

$$\mathcal{V}_{vis} = \frac{-4\beta}{Re}\mathrm{Real}\left[\int_0^{R_0}\frac{1}{r^2}u_{\theta,1}u_{r,1}^* r dr + \int_{R_0}^{1}\frac{\mu_2^0}{r^2}u_{\theta,2}u_{r,2}^* r dr\right], \tag{44}$$

$$\mathcal{V}_g = \frac{1}{Re}\left[\int_{R_0}^{1}\frac{\mu_2^{0\prime}}{r}\left(r u_{r,2}u_{r,2}^*\right)' r dr\right] - \frac{1}{Re}\left[\int_{R_0}^{1}\frac{\mu_2^{0\prime}}{r}u_{\theta,2}u_{\theta,2}^* r dr\right], \tag{45}$$

$$\mathcal{B}_r = \frac{1}{Re}\int_{R_0}^{1}\alpha U_{z,2}'\mathrm{Real}\left(\mu u_{r,2}^*\right) r dr \tag{46}$$

$$\mathcal{V}_p = \int_{R_0}^{1}\left(\frac{dP}{dz}u_{z,2}^*\right) r dr, \tag{47}$$

III. RESULTS AND DISCUSSION

In this section, a parametric study is conducted by varying the spanwise wavenumber (β), the Bingham number (Bn), the flow index (n), the interface radius (R_0) and the inverse capillary number (Γ), and the effect of these parameters on the stability behaviour of the flow configuration considered is investigated.

A. Effect of β

The dispersion curves are plotted for both axisymmetric ($\beta = 0$, represented by solid lines with symbols) and the corkscrew mode ($\beta = 1$, dashed line with symbols) for different values of Bn in Fig. 4. The rest of the parameter values are $Re = 200$, $m = 10$, $\Gamma = 5$, $R_0 = 0.6$ and $n = 1$. In the inset of Fig. 4, a zoomed view of the dispersion curves for the corkscrew mode is shown. The annular layer hosts a fully yielded Bingham fluid with $n = 1$ and $m = 10$, such that the viscosity of the annular fluid is higher than that of the core Newtonian fluid. It has been confirmed (but not shown here) that for $Bn = 0$, $m = 1$ and $n = 1$ (i.e. Newtonian fluids with the same viscosity in both the layers), which corresponds to the Hagen-Poiseuille flow in a pipe, the growth rate is negative, thus validating the prediction that pipe flow is always stable linearly [40].

The Bingham number has an interesting influence on the growth rates of the unstable modes. While it enhances the maximum growth rate of the axisymmetric mode ($\beta = 0$) as Bn increases; it plays a reversed role on the corkscrew mode ($\beta = 1$). The growth rates are positive for both $\beta = 0$ and $\beta = 1$ in the window of the wave numbers considered, where each of these modes exist, but the growth rate is higher for the axisymmetric mode than that of the corkscrew mode. This indicates that the axisymmetric mode is the most unstable mode for this set of parameters considered. This is in contrast to the role of Bn on the stability characteristics observed in case of miscible core-annular configuration with a Newtonian fluid as the core and a Bingham fluid as the annular fluid [32], where the corkscrew mode is the dominant unstable mode when the annular fluid is more viscous than the core fluid.

The behaviour of the axisymmetric ($\beta = 0$) mode and the swirling mode ($\beta = 1$) was also discussed in Refs. [21, 26, 43] for Newtonian fluids. In miscible core-annular systems, both that the axisymmetric ($\beta = 0$) mode and the swirling mode ($\beta = 1$) become the most dominant mode depending on the viscosity stratification. The axisymmetric (the swirling mode) is most dominant unstable mode when the viscosity decreases (increases) as we move from the centreline towards the wall of the pipe [26, 43]. On the other hand, in case of interfacial (immiscible) core-annular systems, axisymmetric disturbances are always the most unstable kind [21].

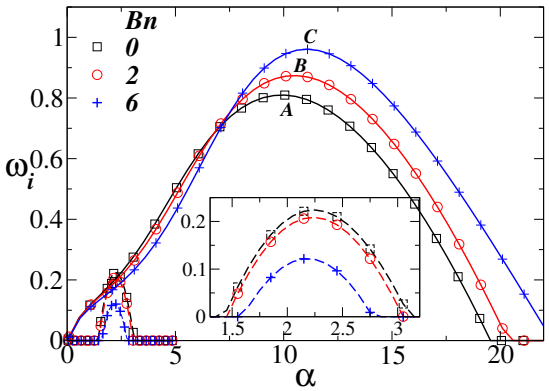

FIG. 4: Effect of β on the the dispersion curves (ω_i versus α) for different values of Bn. Dashed lines with symbols: $\beta = 1$ and solid lines with symbols: $\beta = 0$. The inset is the zoomed view for $\beta = 1$. The rest of the parameter values are $Re = 200$, $m = 10$, $\Gamma = 5$, $R_0 = 0.6$ and $n = 1$. The values of α at points 'A', 'B' and 'C' are 9.8, 10.5 and 11.0, respectively.

When $Bn = 0$ and $n = 1$ with $m = 10$, the viscosity stratified two-layer flow of Newtonian fluids in a core-annular set up is realised and the flow is linearly unstable (thus validating Yih's conclusion for the viscosity stratified flow [15]) to both axisymmetric and corkscrew modes, again with growth rate for $\beta = 0$ higher than that for $\beta = 1$. The bandwidth of the unstable wave numbers increases (decreases) with the increase in Bn for axisymmetric (corkscrew) mode. Instabilities of the corkscrew mode prevails for small wave numbers with small positive growth rates, but those are pushed to short-wave modes with larger growth rates for axisymmetric mode. Also, it has been observed (but not shown) that the growth rates are negative for $\beta = 2$ indicating that the flow is stable for $\beta = 2$; thus it has not been considered further in the present study.

In what follows, we provide a comprehensive description of the temporal linear stability analysis of the pressure-driven core-annular flow of a Newtonian core and non-Newtonian annular fluid whose rheological behaviour is described by the Herschel-Bulkley model. Our goal is to understand how the interfacial instabilities in the system are influenced by the ratio of the yield stress to the viscous stress, i.e. the Bingham number, the viscosity stratification, the wall shear rate and the geometry of the yielded region.

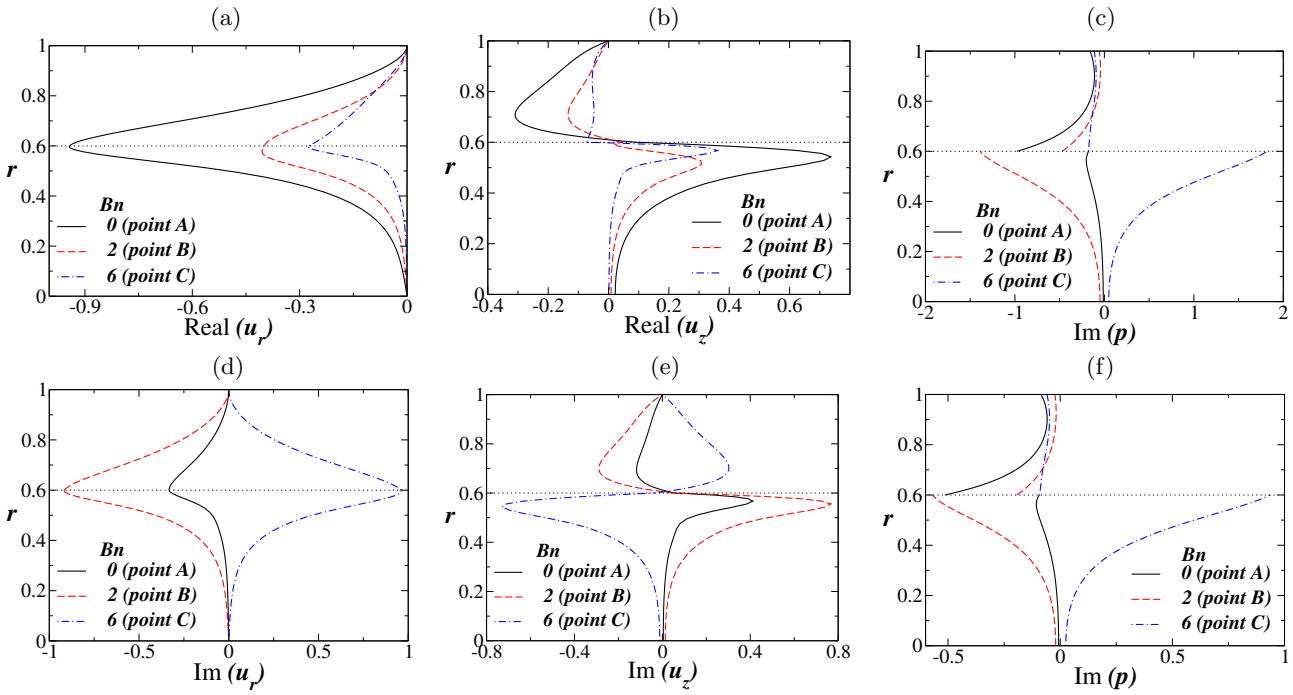

FIG. 5: Profiles of (a,b,c) the real part and (d,e,f) imaginary part of the eigenfunctions u_r, u_z and p associated with the most unstable modes for $\beta = 0$ at points designated by points 'A', 'B' and 'C' in Fig. 4 for $Bn = 0$, 2 and 6, respectively. Note that u_θ is zero as $\beta = 0$. The interface (dotted line) is at $R_0 = 0.6$. The rest of the parameters are the same as those used to generate Fig. 4.

Fig. 5 shows the influence of the Bingham number on the structure of the physical perturbations. The real and the imaginary parts of the eigenfunctions, u_r, u_z and p of the most dominant mode as a function of the radial coordinate for points A, B and C in Fig. 4, at which the growth rate is maximum for $Bn = 0$, 2 and 6, respectively, are presented in Figs. 5(a,b,c) and Figs. 5(d,e,f), respectively. The axial wave numbers, α at which the maximum ω_i ($\omega_{i,max}$) occurs for $Bn = 0$, 2 and 6 are 9.8, 10.5 and 11.0, respectively. It can be seen that, for each Bn, the real part of the perturbation eigenfunction, u_r decreases in the Newtonian core from zero at the centreline to a minimum value attained at the interface and then its gradually increases in the annular region, to become zero at the wall of the pipe. The imaginary part of u_r has a similar behaviour for smaller Bn, but at $Bn = 6$, it is positive in both the layers, increases in the Newtonian core from zero at the centreline and then decreases in the non-Newtonian layer to become zero at the wall. As Bn increases, the values of the imaginary part of u_r at the interface increase monotonically. For $Bn = 0$, the imaginary part of u_r is close to zero near the centreline and zero at the wall. The real part of the perturbation eigenfunction of the axial velocity u_z is negative in the annular region but is positive in the core and the maximum is attained near the interface in the core region for all the Bn values considered. A close look reveals that the real part of u_z is very small at a higher Bn, whereas this is so at a smaller Bn for imaginary u_z. An important observation from the plots in Fig. 5 is that the maximum and minimum values of the real or imaginary part of u_r, u_z and p are attained in a region close to the interface, where the exchange of energy between the basic flow and the perturbations occurs and this is influenced by the changes in Bn.

The physical mechanism that is responsible for the above trend in the growth rates of axisymmetric modes with the increase in Bn can be understood using the energy budget analysis presented in section II D. The contributions from the energy terms in Eq. (39) to the rate of change of the kinetic energy of the disturbance for points A, B and C in Fig. 4 are presented in Table I. For all the values of Bn considered, the energy due to the mean viscosity gradient in the radial direction (B_r) is negligibly small and that in the axial direction is zero. The 'Reynolds stress' contribution denoting the rate of energy transfer from the basic flow to the perturbations is positive and decreases with the increase in Bn. The rate of work done at the interface by the interfacial waves (I) is positive and decrease with the increase in

Point	$\mathcal{P}$	$\mathcal{D}$	$\mathcal{I}$	$\mathcal{V}_{vis}$	$\mathcal{V}_g$	$\mathcal{B}_r$	$\mathcal{B}_z$	$\mathcal{V}_p$
A	0.275	-3.061	2.024	0.0	0.0	0.0	0.0	-0.238
B	0.001	-1.785	1.023	0.0	-0.002	-0.004	0.0	-0.0007
C	0.0008	-0.016	1.037	0.0	-0.009	-0.001	0.0	-0.0002

TABLE I: The contributions from the energy terms in Eq. (39) for the points 'A', 'B' and 'C' in Fig. 4.

Bn. The viscous dissipation of the perturbation energy (D) is negative. The net contribution from P, I and D to the perturbation kinetic energy decreases with the decrease in Bn for the axisymmetric mode, resulting in destabilisation with the increase in Bn. In other words, inspite of the decrease in the total positive contribution from P and I as Bn increases, there is destabilisation due to the decrease in the total viscous dissipation.

B. Effect of Bn

Keeping the other parameters the same as in Fig. 4, the effects of Bn have been studied at a smaller Reynolds number, $Re = 50$ in Fig. 6 for the axisymmetric mode ($\beta = 0$). For any Bn considered, the growth rate is positive, but is significantly reduced as compared to Fig. 4 for which $Re = 200$, thereby stabilising the short waves. We see a non-monotonic behaviour in the dispersion curves for different values of Bn. It can be seen that as Bn increases from $Bn = 0$ to 10, the maximum value of ω_i decreases, but the window of the unstable wave numbers widens; with further increase in Bn ($Bn = 12$), the maximum value of ω_i increases and is more than that for $Bn = 0$. The dispersion curves for larger values of Bn ($Bn = 10$, $Bn = 12$) display two peaks each, one near $\alpha \approx 10$ associated with the maximum growth rate and the other one is at a smaller wave number.

It is possible to understand the physical mechanism of this behaviour of the axisymmetric mode when $Re = 50$ from the energy budget details presented in Table II for points 'A' ($\alpha = 3.5$), 'B' ($\alpha = 4.0$), 'C' ($\alpha = 7.2$) and 'D' ($\alpha = 8.5$) marked on the dispersion curves in Fig. 6 for $Bn = 0$, 5, 10 and 12, respectively. Comparing the contributions of different energy terms at point 'A' in Fig. 4 and Fig. 6 corresponding to $Bn = 0$ (viscosity-stratified core-annular flow with a highly viscous Newtonian fluid in the annular layer; $m = 10$), we infer that the contributions for $Re = 50$ (Table II) are very much reduced (except for the rate of work done by the pressure gradient which is positive for $Re = 50$) as compared to those for $Re = 200$ (Table I). This is responsible for a net reduction in ω_i when $Re = 50$ at point 'A'. As Bn increases to $Bn = 5$, while the positive contribution from $\mathcal{P} + \mathcal{I}$ decreases, the net contribution from $\mathcal{P}$, $\mathcal{I}$ and $\mathcal{D}$ increases resulting in a decrease in the growth rate for $Bn = 5$. However, as Bn increases from $Bn = 10$ to $Bn = 12$, the contributions from $\mathcal{P} + \mathcal{I}$ increases, the viscous dissipation is more negative at point 'D' than at point 'C', causing the energy growth to increase at point 'D'.

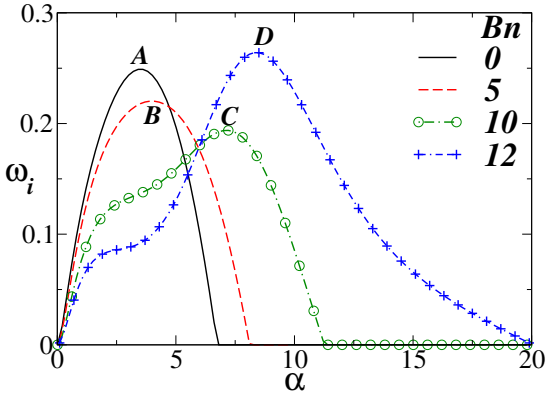

FIG. 6: Effect of Bn on the the dispersion curves (ω_i versus α) for $R_0 = 0.6$. The rest of the parameter values are $Re = 50$, $m = 10$, $r = 1$, $\Gamma = 5$, $\beta = 0$ and $n = 1$. The values of α at points 'A', 'B', 'C' and 'D' are 3.5, 4.0, 7.2 and 8.5, respectively.

The profiles of the real parts and the imaginary parts of the eigenfunctions u_r, u_z and p corresponding to the most unstable axisymmetric mode ($\beta = 0$) for $Bn = 0$, 5, 10 and 12 at the points marked as 'A', 'B', 'C' and 'D' in Fig. 6 are presented in Figs. 7(a,b,c) and Figs. 7(d,e,f), respectively. The other parameter values are the same as those in Fig. 6. The amplitudes of the disturbances of the radial velocity u_r (axial velocity u_z) are positive in both the layers (negative in the core and positive in the annular layer) for $Re = 50$ (Figs. 7a,b), whereas at a higher value of

Point	$\mathcal{P}$	$\mathcal{D}$	$\mathcal{I}$	$\mathcal{V}_{vis}$	$\mathcal{V}_g$	$\mathcal{B}_r$	$\mathcal{B}_z$	$\mathcal{V}_p$
A	0.0012	-0.0088	1.004	0.0	0.0	0.0	0.0	0.0032
B	0.0005	-0.0045	1.003	0.0	0.0004	-0.0006	0.0	0.0011
C	0.0001	-0.005	0.984	0.0	-0.006	-0.004	0.0	-0.001
D	0.0001	-0.005	1.022	0.0	-0.014	-0.004	0.0	0.0004

TABLE II: The contributions from the energy terms in Eq. (39) for the points 'A', 'B', 'C' and 'D' in Fig. 6 for $Bn = 0$, 5, 10 and 12, respectively.

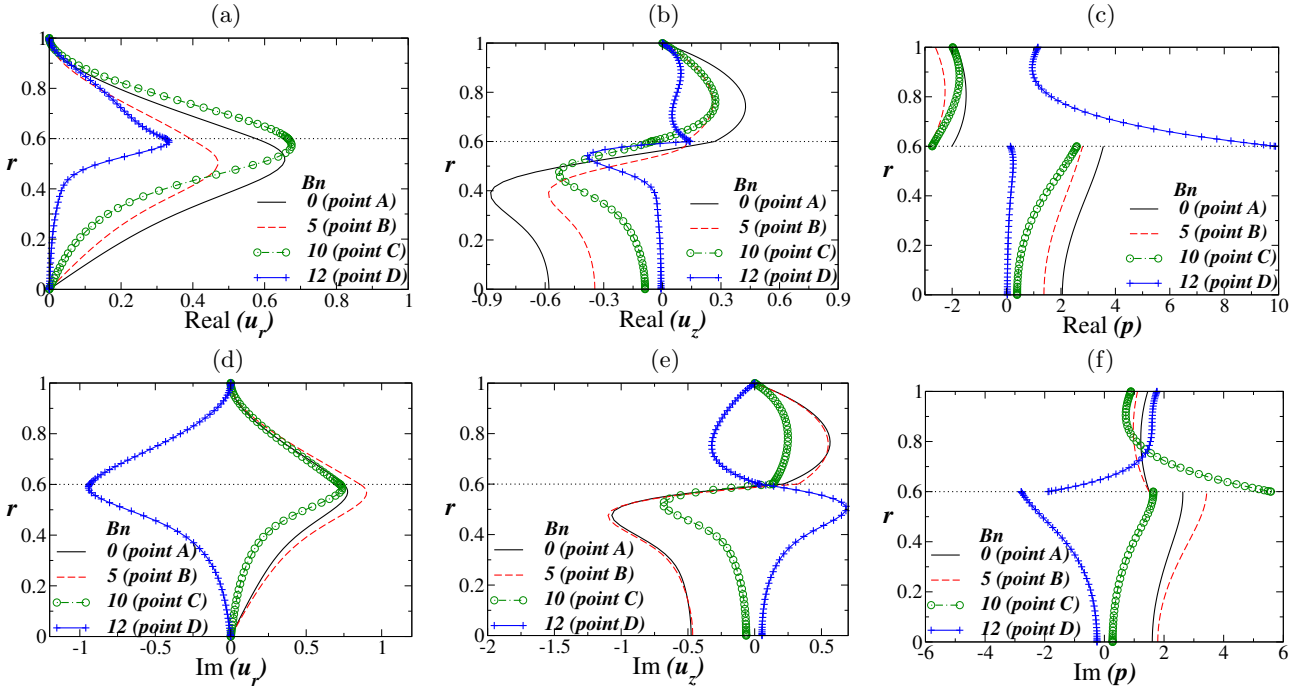

FIG. 7: Profiles of (a,b,c) the real part and (d,e,f) imaginary part of the eigenfunctions u_r, u_z and p associated with the most unstable modes for $\beta = 0$ designated by points 'A', 'B', 'C' and 'D' in Fig. 6 for $Bn = 0$, 5, 10 and 12, respectively. Note that u_θ is zero as $\beta = 0$. The rest of the parameters are the same as those used to generate Fig. 6.

Re ($Re = 200$ in Figs. 5(a,b), the contributions are negative in both the layers (negative in the core and positive in the annular layer). The maximum real value of u_r displays a non-monotonic trend as Bn increases and the maximum values are reached at a radial location near to the interface in the Newtonian core layer. With the increase in Bn, the real (u_r) increases in the core but decreases in the annular layer. While real (u_r) increases in the core to a maximum from values closer to zero near the axis of the pipe, for any Bn considered, it decreases in the non-Newtonian annular layer.

C. Effect of n

The role of flow index n on the linear growth rate, ω_i of the perturbation is depicted in Fig. 8 when $Bn = 10$ and for the axisymmetric mode ($\beta = 0$). The other parameters are fixed as $Re = 50$, $m = 10$ and $\Gamma = 5$. The flow configuration corresponds to a Newtonian core with an entirely yielded non-Newtonian layer of different flow index, n in the annular region. In a window of smaller wavenumbers, the maximum growth increases as n increases, but beyond a cut-off wavenumber, about α_{Bn}, which depends on Bn, an increase in n reduces the growth rate; further, there is a decrease in the bandwidth of unstable wavenumbers, thereby stabilising short waves. There are two peaks in the dispersion curve, showing the existence of another unstable mode at a smaller wave number for every n considered. In order to check the effect of n without the yield stress, we have performed the stability analysis for low values of Bn ($Bn = 0.01$) keeping the rest of the parameters the same as Fig. 8. Figs. 9(a) and (b) show the dispersion curves for different values of n for $\Gamma = 5$ and $\Gamma = 0.01$, respectively. Note that $\Gamma = 0.01$ represents a situation where fluids are immiscible, but have negligible surface tension. We observe that increasing the value of n stabilises the flow, but

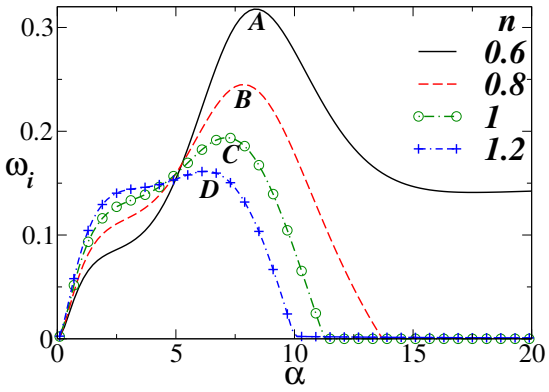

FIG. 8: Effect of n on the the dispersion curves (ω_i versus α) for $R_0 = 0.6$. The rest of the parameter values are $Re = 50$, $m = 10$, $r = 1$, $\Gamma = 5$, $\beta = 0$ and $Bn = 10$. The values of α at points 'A', 'B', 'C' and 'D' are 8.3, 7.9, 7.1 and 6.3, respectively.

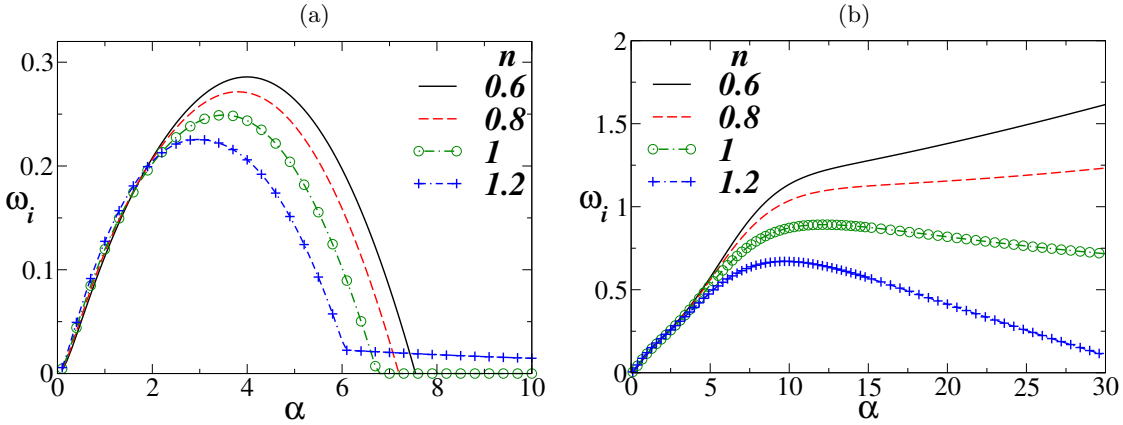

FIG. 9: Effect of n on the the dispersion curves (ω_i versus α) for $Bn = 0.01$: (a) $\Gamma = 5.0$ and (b) $\Gamma = 0.01$. The rest of the parameter values are $R_0 = 0.6$, $Re = 50$, $m = 10$, $r = 1$ and $\beta = 0$ (the same as Fig. 8).

does not show the indication of the second unstable mode as seen in Fig. 8 at low wavenumber region. Thus, we can can conclude that the behaviour observed in Fig. 8 is due to the yield stress effect of the annular fluid.

Inspection of various contributions to the disturbance kinetic energy obtained from the energy budget analysis reveals that $\mathcal{P}$ is not affected by the change in n, but $\mathcal{I}$ decreases as n increases. The negative contributions from $\mathcal{D}$, $\mathcal{V}_g$ and $\mathcal{B}_r$ are small as compared to the positive contribution from $\mathcal{P}$+$\mathcal{I}$. The decrease in the maximum growth rate as n increases (at points 'A', 'B', 'C' and 'D' in Fig. 8) may be attributed to the decrease in $\mathcal{P}$+$\mathcal{I}$ (as seen from Table III) as n increases.

Point	$\mathcal{P}$	$\mathcal{D}$	$\mathcal{I}$	$\mathcal{V}_{vis}$	$\mathcal{V}_g$	$\mathcal{B}_r$	$\mathcal{B}_z$	$\mathcal{V}_p$
A	0.0001	-0.006	1.024	0.0	-0.016	-0.004	0.0	0.001
B	0.0001	-0.008	1.015	0.0	-0.145	-0.004	0.0	0.022
C	0.0001	-0.005	0.984	0.0	-0.006	-0.004	0.0	-0.001
D	0.0001	-0.01	0.970	0.0	-0.01	-0.006	0.0	-0.004

TABLE III: The contributions from the energy terms in Eq. (39) for the points 'A', 'B', 'C' and 'D' in Fig. 8 for $n = 0.6$, 0.8, 1 and 1.2, respectively.

The structure of perturbation eigenfunctions, for different values of n associated with points 'A', 'B', 'C' and 'D' in Fig. 8, presented in Fig. 10 reveals that there is a decrease (increase) in the real (imaginary) part of the radial velocity of the disturbance (u_r) at the interface as n increases. However, the real and imaginary parts of the axial velocity of the disturbance (u_z) display a non-monotonic behaviour in both the layers as n increases. The maximum and minimum values are attained near the interface. At any radial location in the annular region, the real part of the pressure perturbation decreases with the increase in n, but in the Newtonian core, it displays a non-monotonic trend.

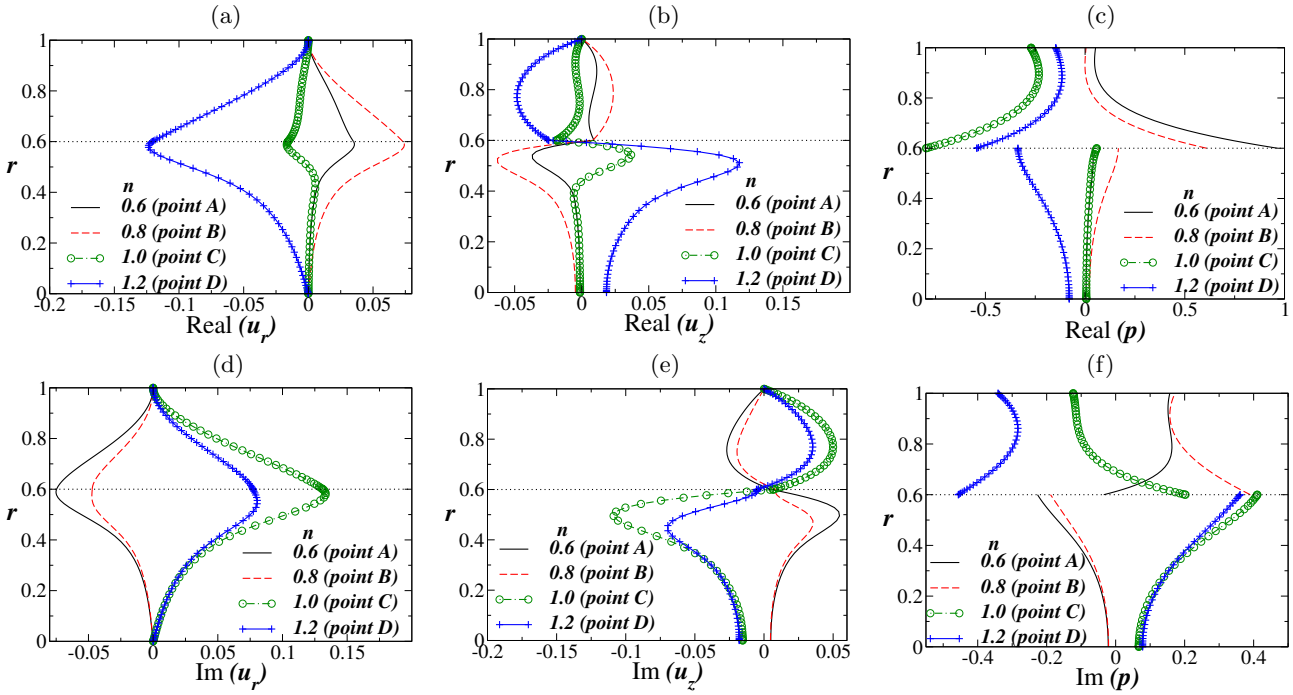

FIG. 10: Profiles of (a,b,c) the real part and (d,e,f) imaginary part of the eigenfunctions u_r, u_z and p associated with the most unstable modes for $\beta = 0$ designated by points 'A', 'B', 'C' and 'D' in Fig. 8 for $n = 0.6$, 0.8, 1 and 1.2, respectively. Note that u_θ is zero as $\beta = 0$. The rest of the parameters are the same as those used to generate Fig. 8.

A reverse scenario is observed for the imaginary part of the pressure perturbation in the two layers as n increases.

D. Effect of R_0

As discussed above, we observe the appearance of another peak at a small wavenumber with a smaller growth rate as compared to the most dominating peak in the dispersion curves for the axisymmetric mode when $R_0 = 0.6$ at a higher value of Bn in Fig. 6 for $n = 1$ and in Fig. 8 for both $n < 1$ and $n > 1$. Thus it is of interest to see what happens as we decrease R_0, i.e. as the interface is moved towards the axis of the pipe. This corresponds to having a flow configuration with a thicker annular fully yielded non-Newtonian fluid with a Newtonian core. The dispersion curves obtained for different values of R_0 are displayed in Fig. 11, when $m = 10$, $Re = 50$, $\Gamma = 5$, $n = 0.6$ and $Bn = 10$ for the axisymmetric mode ($\beta = 0$).

It can be seen in Fig. 11(a) that as the thickness of the core increases (i) the bandwidth of the unstable wavenumbers increases, (ii) destabilises the short waves, (iii) the growth rate displays a non-monotonic behaviour and (iv) the growth rate is dominant for a configuration with equal thickness of the core layer and the annular layer. Further, increasing the thickness of the shear thinning Bingham fluid layer in the annular region (which corresponds to decreasing R_0) increases (decreases) the basic state velocity at the centerline (at the interface), and decreases the velocity gradient of the basic flow in this layer (in the Newtonian core) as is evident in Figs. 11(b) and (c), respectively. Also there is a reduction in the velocity gradient at the interface as R_0 increases and this corresponds to the reduction in the transfer of momentum in the transverse direction. As a result, there is an enhancement in the velocity difference near the wall of the pipe which leads to an increase in the magnitude of the shear stress at the wall. This is a desirable property of a high shear stress fluid near the wall; this aids in surface cleaning in the case of filtration systems or heat exchangers.

The influence of the location of the interface on the maximum growth rate (ω_{max}) for the axisymmetric mode ($\beta = 0$) is displayed in Figs. 12(a) and (b) for different values of Bn with $n = 1$ and different values of n with $Bn = 10$, respectively. The rest of the parameter values are $Re = 50$, $m = 10$, and $\Gamma = 5$. Fig. 12(a) shows that ω_{max} increases as the interface is shifted towards the wall; attains a maximum and then with further increase in R_0, ω_{max} begins to decrease. This suggests that as the Bingham annular layer becomes thinner, there is a reduction in the maximum linear growth rate, thus stabilising the flow configuration. Therefore, a thinner non-Newtonian fluid in the annular region serves as a lubricating fluid. As Bn increases one requires the location of the interface to be much

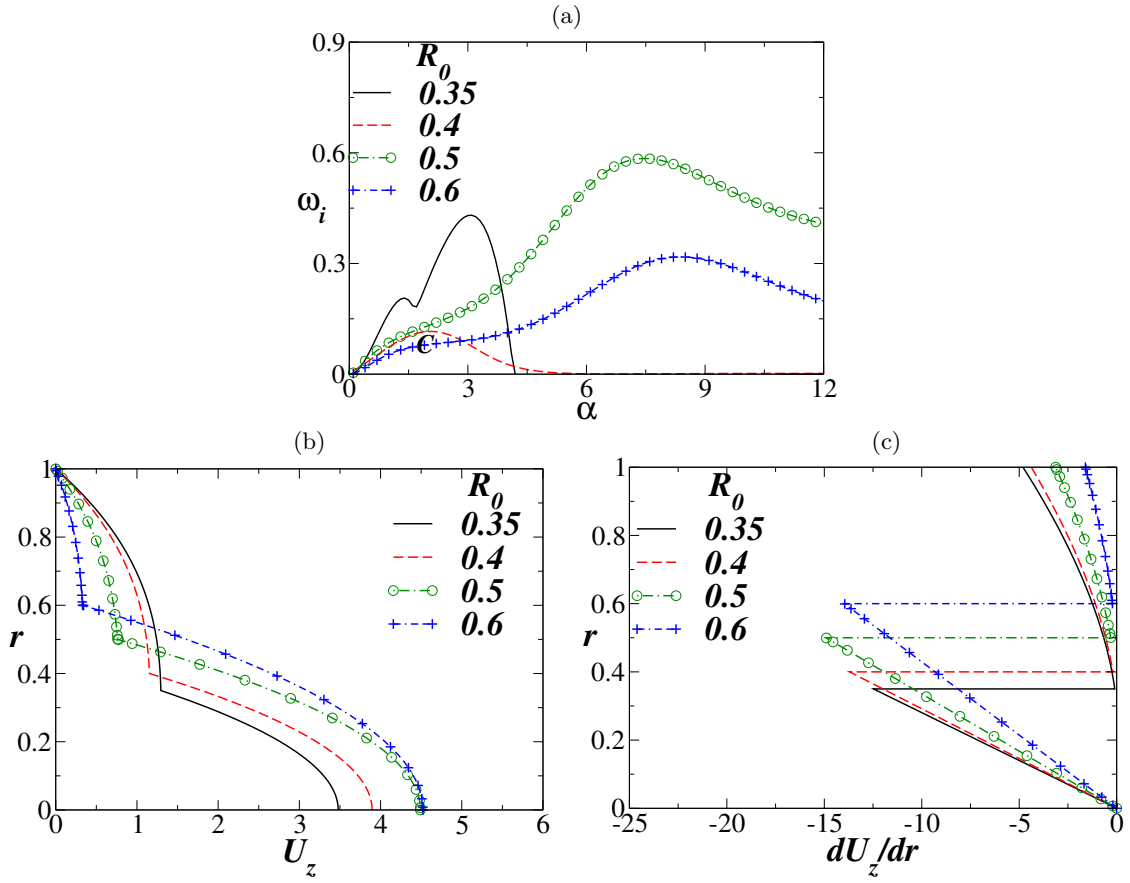

FIG. 11: (a) Appearance of another pick in the dispersion curve at low R_0. The rest of the parameter values are $Re = 50$, $m = 10$, $r = 1$, $\Gamma = 5$, $\beta = 0$, $n = 0.6$ and $Bn = 10$. (b) U_z versus r and and (c) dU_z/dr versus r for different values of R_0.

closer to the wall for this stabilisation to be achieved (see the curves for $Bn = 5$ and 10 in Fig. 12(a)).

Note that beyond $R_0 \approx 0.65$ in Fig. 12(a), ω_{max} increases sharply for $Bn = 12$ after which the velocity profile becomes unphysical due to either static Bingham fluid layer or due to the presence of an unyielded region at the interface for this set of parameters considered. When $Bn = 0$, the flow configuration hosts a high viscous Newtonian fluid in the annular region (similar to Yih's analysis [15]). The flow system remains unstable for a wide range of R_0 and a layer of Newtonian fluid in the annular region much thicker than that for a non-Newtonian annular fluid is required to stabilise this core annular configuration. Similar conclusions are valid in the variation of ω_{max} versus R_0 as the flow index n is varied with $Bn = 10$, as is evident from Fig. 12(b).

E. Effect of Γ

In Fig. 13, the variations of ω_i versus α for different values of the inverse capillary number are shown for $Re = 50$, $m = 10$, $r = 1$, $Bn = 10$, $R_0 = 0.6$, $\beta = 0$ and $n = 1$. It can be seen that the axisymmetric mode ($\beta = 0$) is stabilised (decrease in maximum growth rate) by an increase in surface tension for the core-annular configuration with an annular layer hosting a high viscous ($m = 10$) Bingham fluid ($Bn = 10$, $n = 1$) thinner than the core layer ($R_0 = 0.6$). This finding is consistent with that of Ref. [46] who showed that increasing the inverse capillary number stabilises the short waves in a three-layer channel flow.

IV. CONCLUSIONS

We investigate the linear instability in pressure-driven core-annular flow of a non-Newtonian fluid, characterised by the Herschel-Bulkley rheological modal, hosted in the annular region and a Newtonian fluid occupying the core region of a cylindrical pipe. The fluids are assumed to be immiscible and incompressible having the same density. The

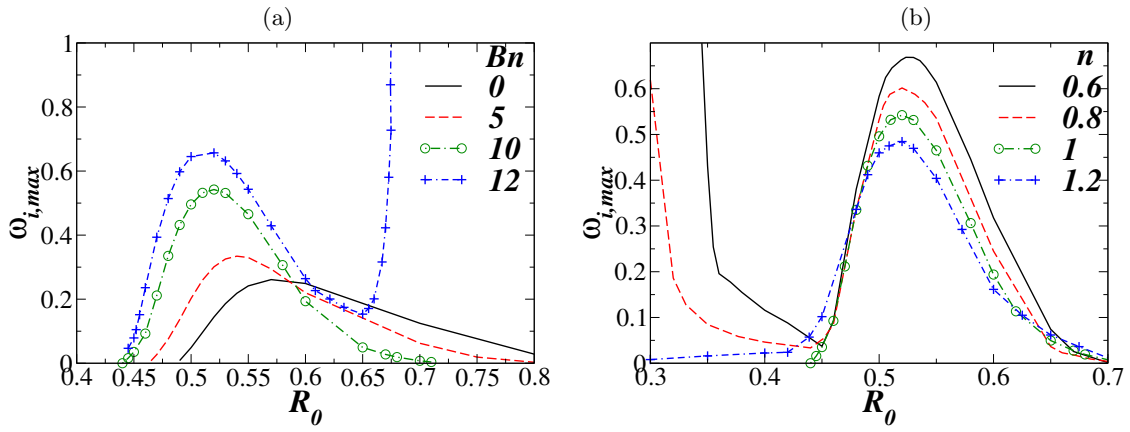

FIG. 12: The variations of $\omega_{i,max}$ versus R_0 (a) for different values of Bn for $n = 1$, and (b) for different values of n for $Bn = 10$. The rest of the parameter values are $Re = 50$, $m = 10$, $r = 1$, $\Gamma = 5$, $\beta = 0$ and $n = 1$.

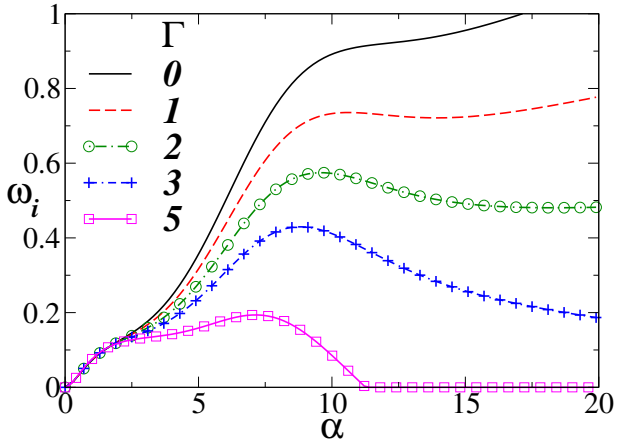

FIG. 13: Effect of Γ on the the dispersion curves (ω_i versus α). The rest of the parameter values are $Re = 50$, $m = 10$, $r = 1$, $Bn = 10$, $R_0 = 0.6$, $\beta = 0$ and $n = 1$.

dimensionless parameters influencing the flow are the Bingham number (Bn), the flow index (n), the interface radius (R_0) and the inverse capillary number (Γ). The effect of these parameters on the instability characteristics of the flow is investigated, and an energy budget analysis is conducted to explain the physical mechanism of the instability observed. Although the presence of a plug zone is the characteristic feature of a viscoplastic fluid that differentiates it from the other class of non-Newtonian fluids, we have explored only those parameter values for which the Herschel-Bulkley is fully yielded; the critical condition for which the entire non-Newtonian fluid is yielded is derived as Eq. (12). Our study will therefore be of special interest to those interested in the transient growth of disturbances and their nonlinear growth in core-annular system.

In contrast to the corkscrew mode ($\beta = 1$) becoming the most dominant unstable mode when the annular fluid is more viscous than the core fluid in miscible core-annular flow of Newtonian and Bingham fluids and in double-diffusive miscible core-annular pipe flow of Newtonian fluids, we found that the axisymmetric mode ($\beta = 0$) is the dominant unstable mode in case of core-annular pipe flow of immiscible fluids separated by a sharp interface, as considered in the present study. This is true irrespective of whether the annular fluid is Newtonian or non-Newtonian and for all the parameters considered in the present work.

For axisymmetric disturbances in concentric stratified flow of two Newtonian fluids, the flow is unstable when the annular fluid is more viscous than the core fluid [47]. This scenario is also observed when the annular layer hosts a yield-stress fluid (Herschel-Bulkley rheological modal) with higher viscosity that the Newtonian core and the stability behaviour is highly dependent on Bn, n, m and R_0. We found that increasing Bn has a non-monotonic effect on the growth rate of the axisymmetric mode. We observe that two dominant modes for high Bn at $R_0 = 0.6$; one is associated with the mode with the highest growth rate for an intermediate axial wave number (α) and the other one with a smaller growth rate at a lower value of α.

By varying R_0, we observed that increasing the thickness of the core fluid increases the bandwidth of the unstable wavenumbers and destabilises the short waves; however, displays a non-monotonic trend in the growth rate curves. Inspection of basic state velocity profiles reveals that increasing the thickness of the Herschel-Bulkley annular fluid decreases the velocity gradient of the basic flow in this layer, which in turn reduces the transfer of momentum in the transverse direction, and thus expected to stabilise the flow for high Bn. Therefore, a thinner non-Newtonian fluid in the annular region serves as a lubricating fluid. As expected, we found that increase in surface tension stabilised the short waves.

The physical mechanism responsible for instability in miscible flow system discussed in Sahu [32] and the immiscible flow configuration considered in the present study are different as revealed by the energy budget analysis. While in miscible flow systems, the energy due to the gradient of viscosity perturbation in the radial direction and the transfer of energy from the basic flow to the perturbation via the "Reynolds stress" term were responsible for the instability, in the immiscible flow configuration, inspite of the total positive contributions from both the rate of energy transfer from the basic flow to the perturbation and the rate of work done at the interface due to interfacial forces, the decrease in the total viscous dissipation is found to be responsible for the destabilisation observed. Further, the rate of work done by the gradient of viscosity perturbation in the radial direction (in the immiscible system) is negligible in contrast to its role for destabilisation in the case of miscible flow system. In the immiscible core-annular flow, a positive contribution of the energy transfer arises from the rate of work done at the interface by the interfacial forces. This may be attributed to the difference in the trends observed in the miscible and immiscible systems.

Acknowledgement: The author thanks Department of Science & Technology, India for providing financial support through the grant number, MTR/2017/000029.

[1] C. Nouar and I. A. Frigaard, "Nonlinear stability of Poiseuille flow of a Bingham fluid: theoretical results and comparison with phenomenological criteria," J. Non-Newtonian Fluid Mech. **100**, 127 (2001).
[2] M. A. Moyers-Gonzalez, I. A. Frigaard, and C. Nouar, "Nonlinear stability of a visco-plastically lubricated viscous shear flow," J. Fluid Mech. **506**, 117 (2004).
[3] S. Hormozi, K. Wielage-Burchard, and I. A. Frigaard, "Entry, start up and stability effects in visco-plastically lubricated pipe flows," J. Fluid Mech. **673**, 432 (2011).
[4] M. Moyers-Gonzalez, I. A. Frigaard, and C. Nouar, "Stable two-layer flows at all Re; visco-plastic lubrication of shear-thinning and viscoelastic fluids," J. Non-Newtonian Fluid Mech. **165**, 1578 (2010).
[5] I. Frigaard and C. Nouar, "On three-dimensional linear stability of Poiseuille flow of Bingham fluids," Phys. Fluids **15 (10)**, 2843 (2003).
[6] P. G. Drazin and W. H. Reid, *Hydrodynamic stability* (Cambridge University Press, Cambridge, 1985).
[7] K. C. Sahu, H. Ding, P. Valluri, and O. K. Matar, "Linear stability analysis and numerical simulation of miscible channel flows," Phys. Fluids **21**, 042104 (2009).
[8] K. C. Sahu and O. K. Matar, "Three-dimensional linear instability in pressure-driven two-layer channel flow of a Newtonian and a Herschel-Bulkley fluid," Phys. Fluids **22**, 112103 (2010).
[9] S. Ghosh, R. Usha, and K. C. Sahu, "'Linear stability analysis of miscible two-fluid flow in a channel with velocity slip at the walls," Phys. Fluids. **26**, 014107 (2014).
[10] I. A. Frigaard, S. D. Howison, and I. J. Sobey, "On the stability of Poiseuille flow of a Bingham fluid," J. Fluid Mech. **263**, 133 (1994).
[11] A. Esmael and C. Nouar, "Transitional flow of a yield-stress fluid in a pipe: Evidence of a robust coherent structure," Phys. Rev. E. **77**, 057302 (2008).
[12] R. Liu and Q. S. Liu, "Non-modal stability in Hagen-Poiseuille flow of a Bingham fluid," Phys. Fluids **26**, 014102 (2014).
[13] H. Bentrad *et al.*, "Energy growth in Hagen–Poiseuille flow of Herschel–Bulkley fluid," J. Non-Newtonian Fluid Mech. **241**, 43 (2017).
[14] R. Liu, Z. Ding, and K. X. Hu, "Stabilities in plane Poiseuille flow of Herschel–Bulkley fluid," J. Non-Newtonian Fluid Mech. **251**, 132 (2018).
[15] C. S. Yih, "Instability due to viscous stratification," J. Fluid Mech. **27**, 337 (1967).
[16] M. J. South and A. P. Hooper, "Linear growth in two-fluid plane Poiseuille flow," J. Fluid Mech. **381**, 121 (1999).
[17] S. G. Yiantsios and B. G. Higgins, "Linear stability of plane Poiseuille flow of two superposed fluids," Phys. Fluids **31**, 3225 (1988).
[18] S. G. Yiantsios and B. G. Higgins, "Numerial solution of eigenvalue problems using the compound matrix-method," J. Comp. Phys. **74**, 25 (1988).
[19] A. P. Hooper and R. Grimshaw, "Nonlinear instability at the interface between two viscous fluids," Phys. Fluids **28(1)**, 37 (1985).
[20] K. C. Sahu, P. Valluri, P. D. M. Spelt, and O. K. Matar, "Linear instability of pressure-driven channel flow of a Newtonian

and Herschel-Bulkley fluid," Phys. Fluids **19**, 122101 (2007).
[21] R. Govindarajan and K. C. Sahu, "Instabilities in viscosity-stratified flows," Ann. Rev. Fluid Mech. **46**, 331 (2014).
[22] E. Lajeunesse, J. Martin, N. Rakotomalala, and D. Salin, "3D instability of miscible displacements in a Hele-Shaw cell," Phys. Rev. Lett. **79**, 5254 (1997).
[23] J. Scoffoni, E. Lajeunesse, and G. M. Homsy, "Interface instabilities during displacement of two miscible fluids in a vertical pipe," Phys. Fluids **13**, 553 (2001).
[24] B. Selvam, L. Talon, L. Lesshafft, and E. Meiburg, "Convective/absolute instability in miscible core-annular flow. Part 2. Numerical simulations and nonlinear global modes," J. Fluid Mech. **618**, 323 (2009).
[25] M. d'Olce *et al.*, "Pearl and mushroom instability patterns in two miscible fluids core annular flows," Phys. Fluids **20**, 024104 (2008).
[26] B. Selvam, S. Merk, R. Govindarajan, and E. Meiburg, "Stability of miscible core-annular flows with viscosity stratification," J. Fluid Mech. **592**, 23 (2007).
[27] M. Mishra, A. De Wit, and K. C. Sahu, "Double diffusive effects on pressure-driven miscible displacement flows in a channel," J. Fluid Mech. **712**, 579 (2012).
[28] I. A. Frigaard, "Super-stable parallel flows of multiple visco-plastic fluids," J. Non-Newtonian Fluid Mech. **100**, 49 (2001).
[29] S. Hormozi, K. Wielage-Burchard, and I. A. Frigaard, "Multi-layer channel flows with yield stress fluids," J. Non-Newtonian Fluid Mech. **166**, 262 (2011).
[30] A. Pinarbasi and A. Liakopoulos, "Stability of two-layer Poiseulle flow of Carreau-Yasuda and Bingham-like fluids," J. Non-Newtonian Fluid Mech. **57**, 227 (1995).
[31] K. C. Sahu and O. K. Matar, "Three-dimensional convective and absolute instabilities in pressure-driven two-layer channel flow," Int. J. Multiphase Flow **37**, 987 (2011).
[32] K. C. Sahu, "Linear instability in a miscible core-annular flow of a Newtonian and a Bingham fluid," J. Non-Newtonian Fluid Mech. **264**, 159 (2019).
[33] M. P. Escudier and F. Presti, "Pipe flow of a thixotropic liquid," J. Non-Newtonian Fluid Mech. **62**, 291 (1996).
[34] M. P. Escudier *et al.*, "Observations of asymmetrical flow behaviour in transitional pipe flow of yield-stress and other shear-thinning liquids," J. Non-Newtonian Fluid Mech. **127**, 143 (2005).
[35] J. Peixinho, C. Nouar, C. Desaubry, and B. Théron, "Laminar transitional and turbulent flow of yield stress fluid in a pipe," J. Non-Newtonian Fluid Mech. **128**, 172 (2005).
[36] B. Güzel, T. Burghelea, I. A. Frigaard, and D. M. Martinez, "Observation of laminar–turbulent transition of a yield stress fluid in Hagen–Poiseuille flow," J. Fluid Mech. **627**, 97 (2009).
[37] C. K. Huen, I. A. Frigaard, and D. M. Martinez, "Experimental studies of multi-layer flows using a visco-plastic lubricant," J. Non-Newtonian Fluid Mech. **142**, 150 (2007).
[38] S. Hormozi and I. Frigaard, "Nonlinear stability of a visco-plastically lubricated viscoelastic fluid flow," J. Non-Newtonian Fluid Mech. **169**, 61 (2012).
[39] S. Hormozi, D. M. Martinez, and I. A. Frigaard, "Stable core-annular flows of viscoelastic fluids using the visco-plastic lubrication technique," J. Non-Newtonian Fluid Mech. **166**, 1356 (2011).
[40] P. J. Schmid and D. S. Henningson, *Stability and transition in shear flows* (Springer-Verlag New York, Inc, New York, 2001).
[41] K. C. Sahu and R. Govindarajan, "Stability of flow through a slowly diverging pipe," J. Fluid Mech. **531**, 325 (2005).
[42] C. Canuto, M. Y. Hussaini, A. Quarteroni, and T. Zang, *Spectral Methods in Fluid Dynamics*, 1st ed. (Springer-Verlag, Amsterdam, 1987), pp. 65–70.
[43] K. C. Sahu, "Double-diffusive instability in core–annular pipe flow," J. Fluid Mech. **789**, 830 (2016).
[44] S. Ghosh, R. Usha, and K. C. Sahu, "Double-diffusive two-fluid flow in a slippery channel: A linear stability analysis," Phys. Fluids. **26**, 015412 (2014).
[45] P. A. M. Boomkamp and R. H. M. Miesen, "Classification of instabilities in parallel two-phase flow," Int. J. Multiphase Flow **22**, 67 (1996).
[46] P. R. Redapangu, K. C. Sahu, and S. P. Vanka, "study of pressure-driven displacement flow of two immiscible liquids using a multiphase lattice Boltzmann approach," Phys. Fluids **24**, 102110 (2012).
[47] C. E. Hickox, "Instability due to viscosity and density stratification in axisymmetric pipe flow," Phys. Fluids **14**, 251 (1971).